nature communications

Article

https://doi.org/10.1038/s41467-025-59637-x

Rhythmic radial oxygen loss enhances soil phosphorus bioavailability

Received: 20 March 2025

Accepted: 29 April 2025

Published online: 13 May 2025

Check for updates

Cai Li[1,4], Hu Sheng[1,4], Mengxi Tan[2], Hengyi Dai[2], Xiaolong Wang[1], Huacheng Xu[1], Shiming Ding[3] & Guoqiang Zhao[1]

Phosphorus (P) availability is vital for global primary productivity, yet it is often immobilized in soils by redox-inert crystalline iron (oxy)hydroxides. Here we show that diel radial oxygen loss (ROL) from plant roots induces redox fluctuations in the rhizosphere, activating these iron minerals and enhancing P mobilization. Nighttime reduction and daytime oxidation drive the formation of reactive metastable iron phases (RMPs) on root surfaces, forming a redox-active iron plaque. These RMPs undergo rapid dissolution–reformation cycles, facilitating P transfer from soil to porewater for plant uptake. Using multiple aquatic plants from agriculturally developed regions, we demonstrate that ROL broadly enhances soil P availability. In rice paddies, ROL-activated P release accounts for 8.7% of global P fertilizer input, contributing an estimated economic value of USD 0.52 billion annually. Our findings uncover a previously overlooked redox mechanism by which plants enhance P acquisition, with broad implications for nutrient cycling and agricultural sustainability.

Phosphorus (P) is a critical biogenic element for plant growth, and its bioavailability is a key determinant of plant productivity[1]. In soils, the efficiency of P uptake by plants is closely linked to the chemical forms of P present. Soluble reactive P is highly bioavailable, but this labile fraction usually accounts for less than 6% of the total P in soils[2]. The majority of P is tightly bound to soil minerals or organic compounds as unavailable P, often resulting in P deficiencies that limit plant growth[3]. To thrive in these P-limited environments, plants have developed various adaptive strategies to improve P availability[4]. However, most reported mechanisms for plant activation of immobilized P involve aperiodic processes, such as the secretion of phosphatases[5], mycorrhizal symbiosis[6], the development of complex root architectures[2], and the release of organic acids[7].

Plants primarily absorb P from soils through their rhizomes and roots[6]. The solubilization of P in the rhizosphere plays a crucial role in alleviating P scarcity. One of the key pathways for solubilizing P in soils is the microbial reduction of Fe(III)-(oxy)hydroxides to soluble Fe(II), which releases associated P into the porewater[8]. Notably, P bound to insoluble Fe(III) (oxy)hydroxides represents a major soil P pool, accounting for approximately 30–85% of the total P[9]. However, iron minerals in soils are predominantly found in highly crystalline forms[10,11], which are thermodynamically stable and exhibit low rates and extents of reduction[12,13]. This stability poses a challenge for P mobilization, as these forms of iron are inert and less likely to release associated P[14]. However, the rhythmic radial oxygen loss (ROL) of aquatic plants, such as rice (Oryza sativa L.)[15], may provide a mechanism to overcome this limitation. During the day, photosynthesis raises the partial pressure of oxygen in the lacunae, promoting oxygen diffusion into the rhizosphere. At night, the absence of photosynthesis lowers internal oxygen, creating anoxic conditions that drive microbial reduction processes (e.g., by *Shewanella*)[16]. These diel shifts in ROL give rise to periodic redox fluctuations in the rhizosphere[17]. We wonder whether such circadian ROL-induced redox dynamics could activate thermodynamically stable iron minerals into reactive mineral phases (RMPs), thereby enhancing the accumulation and dissolution of P in the rhizosphere. If confirmed, this could provide a potential pathway to improve P availability in soils (Fig. 1a).

The present study aims to investigate how diel redox fluctuations driven by ROL enhance P bioavailability in the rhizosphere. Using a

[1]State Key Laboratory of Lake and Watershed Science for Water Security, Nanjing Institute of Geography and Limnology, Chinese Academy of Sciences, Nanjing, China. [2]Faculty of Agriculture, Life, and Environmental Sciences, Zhejiang University, Hangzhou, China. [3]School of Energy and Environment, Southeast University, Nanjing, China. [4]These authors contributed equally: Cai Li, Hu Sheng. e-mail: gqzhao@niglas.ac.cn

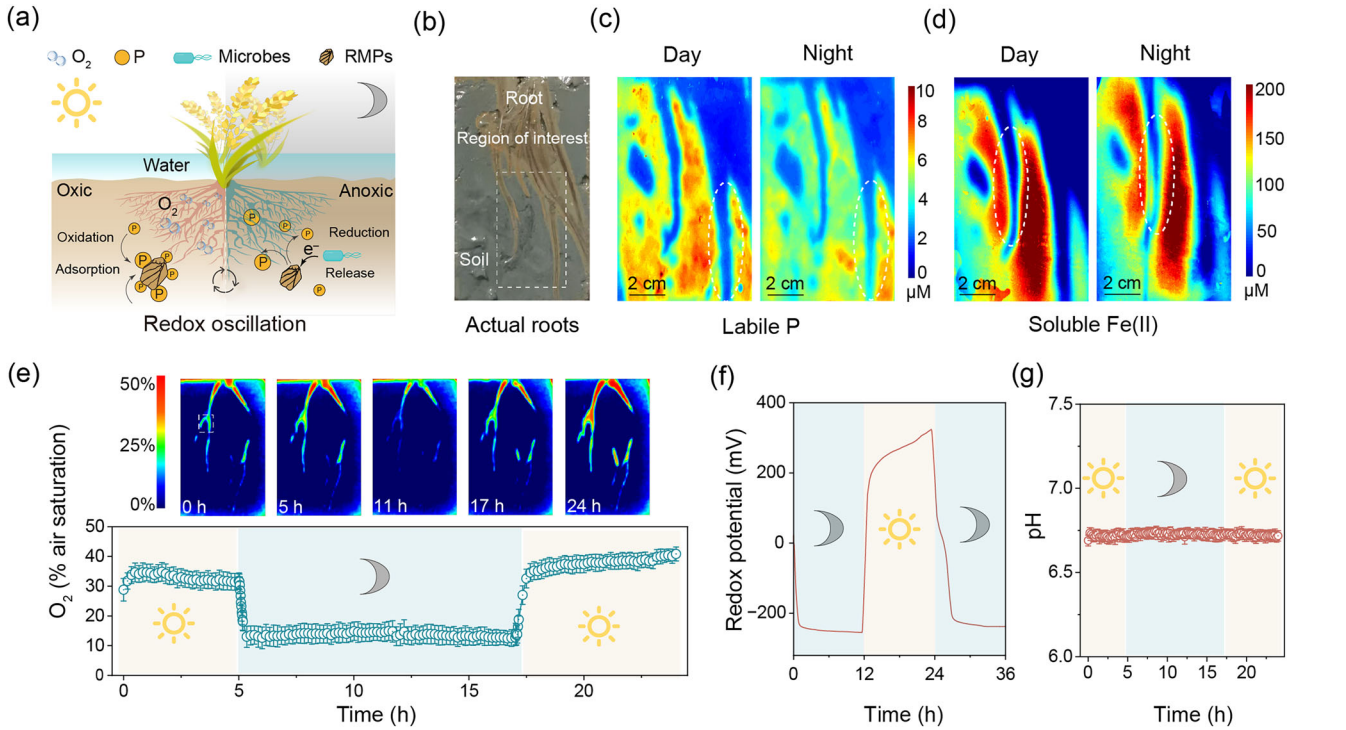

Fig. 1 | Diel fluctuations of P and Fe in the rootzone. a Schematic representation of diel ROL-driven enhancement of P bioavailability via reactive mineral phases (RMPs). **b** Photographic images of roots in the experimental setup. **c**, **d** Visualization of diel fluctuations in labile P and soluble Fe(II) concentrations in the rootzone using a diffusive gel film imaging system. **e**, **f** Diel variations in oxygen content and redox potential in the rootzone. **g** The temporal dynamics of rhizosphere pH. The error bars represent the standard deviations of three replicates. When error bars are not visible, they are contained within the marker symbols.

diffusive gel film imaging system, we observed that Fe around plant roots undergoes cyclic dissolution and reprecipitation, mobilizing soil P into rhizosphere porewater for plant uptake. Electrochemical analyses revealed that these redox fluctuations were mediated by RMPs on root surfaces. Diurnal redox fluctuations were identified as a critical mechanism transforming crystalline Fe minerals into RMPs. We further investigated the generality of circadian ROL in enhancing P availability across diverse soils and plant species and assessed its global economic benefits. These findings uncover a diel ROL-driven mechanism for P mobilization, providing insights into plant strategies to overcome P limitations and informing sustainable agricultural practices.

Results and discussion

Diel ROL-driven fluctuations of P and Fe

We developed a diffusive gel film imaging system to monitor the dissolution of P and Fe in the root-associated zone (Figs. 1b and S1). Seedlings of *Vallisneria natans* H. were transplanted into water-saturated soils in rhizoboxes and cultivated in a greenhouse for one month to establish equilibrium conditions. Diffusive gradients in thin films (DGT) were then attached to the inner walls of the rhizoboxes to track diel variations in labile P near the root zone. During the day, under light exposure, elevated concentrations of labile P (4–8 μM) were observed in the soil surrounding the roots. At night, as oxygen became depleted, stored labile P in the soil dissolved rapidly into rhizosphere porewater (Figs. S2 and S3), leading to a notable decline in soil labile P concentrations (3–6 μM; Fig. 1c). These patterns indicate that diel ROL dynamics effectively drive P fluctuations. Given the critical role of iron minerals in regulating P mobility[18], we simultaneously measured soluble Fe(II) in the root zone using diffusive equilibration in thin films (DET). Consistent with the trends observed for P, soluble Fe(II) accumulated around the roots during the day was released into rhizosphere porewater at night (Figs. 1d and S4). These synchronized diel fluctuations of P and Fe suggest that iron minerals in the rhizosphere may exhibit high redox activity, undergoing rapid redox cycling driven by ROL. Such ROL-induced iron transformations likely mediate the periodic adsorption and release of P, promoting its mobilization and enhancing bioavailability in the rhizosphere.

We propose that, during the day, roots release oxygen into the surrounding rhizosphere, promoting the oxidation of soluble Fe(II) to Fe(III) oxides. These Fe(III) oxides efficiently sequester labile P from soil, forming Fe(III)-associated P. At night, as oxygen levels decline, microbial anaerobic respiration drives the reductive dissolution of Fe(III)-associated P, releasing Fe(II) and P into rhizosphere porewater for root uptake (Fig. 1e, f). In parallel, localized ROL-driven oxidation of Fe(II) and sulfides, combined with root-induced unbalanced cation–anion uptake and organic acid secretion, induces a sustained mild acidification in the rhizosphere[8,9], with slight fluctuations around pH 6.7. (Figs. 1g and S5). This pH reduction enhances P solubilization while mitigating the re-precipitation of Fe(III) and P at the basal leaf meristem, increasing P availability in rhizosphere porewater. Consequently, periodic redox cycles drive iron minerals to function as dynamic shuttles, continuously mobilizing labile P from the soil into rhizosphere porewater, thereby enhancing P bioavailability and supporting plant nutrient uptake.

The presence of RMPs around the roots

To assess whether redox activity is particularly pronounced near roots, we sequentially isolated iron plaques, rhizosphere soil, and bulk soil from the root surface outward (Fig. S6). Electrochemical analyses revealed distinct redox behaviors among these components. Cyclic voltammetry (CV) curves revealed that iron plaque exhibited the highest current, characterized by two distinct reduction peaks. In contrast, rhizosphere soil displayed a lower current with a prominent oxidation peak, while bulk soil showed minimal current and lacked notable redox features (Fig. 2a). These CV results qualitatively indicate that iron plaque possesses the strongest redox activity, followed by

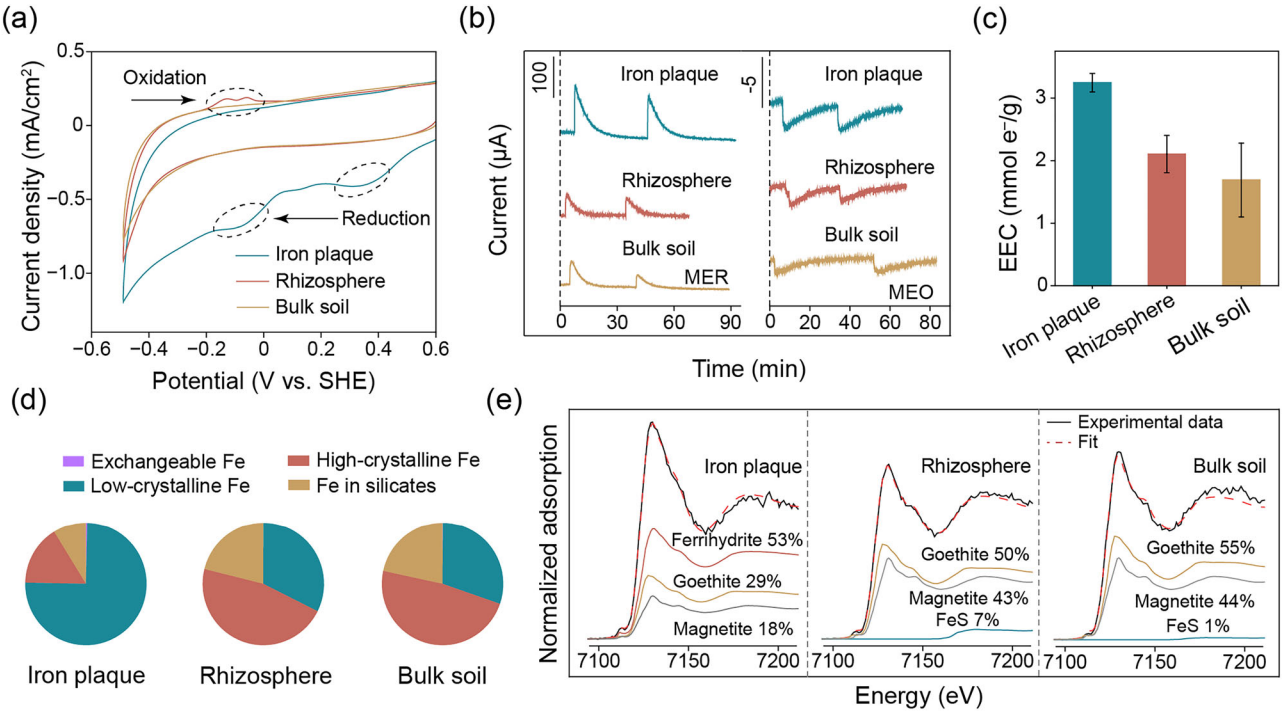

Fig. 2 | Reactive mineral phases (RMPs) formation near roots. **a** Current–potential curves (reported versus the standard hydrogen electrode, SHE) showing redox activity. **b** Mediated electrochemical reduction (MER) and oxidation (MEO) curves, and **c** electron exchange capacity (EEC) measurements of iron plaque, rhizosphere soil, and bulk soil. **d** Iron fractions characterized by sequential chemical extraction. **e** Iron species identified using X-ray absorption spectroscopy. The error bars represent the standard deviations of three replicates. When error bars are not visible, they are contained within the marker symbols.

rhizosphere soil, with bulk soil being largely redox-inactive. The enhanced redox activity of iron plaque was further supported by mediated electrochemical reduction (MER) and oxidation (MEO) analyses, which showed significantly higher currents and two parallel peaks (Fig. 2b). Quantitatively, the electron exchange capacity (EEC) of iron plaque, calculated by integrating the current over time, was 3.2 mmol e^-/g, i.e., 1.6- and 1.8-fold higher than that of rhizosphere soil and bulk soil, respectively (Fig. 2c). These results suggest that the iron plaque closest to the root exhibited the highest redox activity.

Given the close link between the redox properties of iron phases and their morphology, type, and crystallinity[19,20], we further examined the chemical fractions and speciation of iron in root-associated compartments. Sequential chemical extraction showed that the iron plaque contained a markedly higher proportion of low-crystalline iron (74.9% of the total iron) compared to the rhizosphere soil (32.3%) and bulk soil (30.2%) (Figs. 2d and S7). X-ray absorption spectroscopy (XAS) further revealed that these poorly crystalline iron fractions were primarily derived from amorphous ferrihydrite (Fig. 2e), a redox-active, metastable iron mineral with low crystallinity, commonly categorized as RMPs[19,21]. RMPs deviate from the Gibbs free energy minimum for a given atomic composition, reflecting thermodynamic non-equilibrium states[22]. Previous studies have established that highly crystalline iron minerals, such as goethite and magnetite, exhibit greater thermodynamic stability and lower redox activity relative to poorly crystalline ferrihydrite[12,13]. Collectively, these findings suggest that the enhanced redox activity near roots is largely driven by the prevalence of poorly crystalline RMPs.

RMPs as hotspots for rhizosphere P mobilization

DGT coupled with laser ablation–inductively coupled plasma mass spectrometry (LA–ICPMS) is a powerful imaging technique for detecting labile iron in soils and sediments[5]. Notably, the majority of redox-active iron in soils is derived from labile iron[23], which is broadly defined here as RMPs. We employed DGT–LA–ICPMS to map the spatial distribution of RMPs in iron plaque, rhizosphere soil, and bulk soil (Fig. 3a). The analysis revealed that oxygen-releasing root surfaces adsorbed substantial amounts of labile iron, confirming the localized formation of RMPs as iron plaque on the root surface (Fig. 3b, c). These RMPs demonstrated a high phosphate adsorption capacity, accounting for the enrichment of 90% of the phosphate around the roots (Fig. 3d). This pattern aligned with the distribution of reactive iron within the root zone, providing further evidence for the strong phosphate enrichment capability of root-surface-adsorbed RMPs (Fig. 3e).

We further analyzed diel fluctuations of available P in iron plaques, rhizosphere soil, and bulk soil using sodium bicarbonate ($NaHCO_3$, pH 8.5) extraction[24]. Diurnal variations in available P were observed, with the highest concentrations and most pronounced fluctuations occurring in iron plaques, followed by rhizosphere soil. In contrast, the available P in the bulk soil exhibited minimal concentrations and negligible diurnal fluctuations (Fig. 3f). These rhythmic oscillations of available P around the roots were closely tied to the diel redox cycling of RMPs, as evidenced by marked variations in reactive Fe(II) concentrations within the iron plaques (Fig. 3g). By comparison, reactive iron in rhizosphere and bulk soils showed no significant redox fluctuations, likely due to the limited abundance of RMPs and the constrained spatial influence of periodic ROL, which diminishes with distance from the root. Collectively, these findings underscore the role of RMPs closest to the root as critical hotspots for the accumulation and mobilization of P in the root zone, driven by periodic ROL.

ROL-driven redox cycling facilitates RMPs production

We next examined the mechanisms driving rhizosphere RMPs formation. To investigate whether ROL-induced redox fluctuations can activate thermodynamically stable iron minerals in soil to generate RMPs, we selected goethite as a model iron mineral for this study (Fig. S8). Goethite is a highly crystalline and thermodynamically stable

https://doi.org/10.1038/s41467-025-59637-x

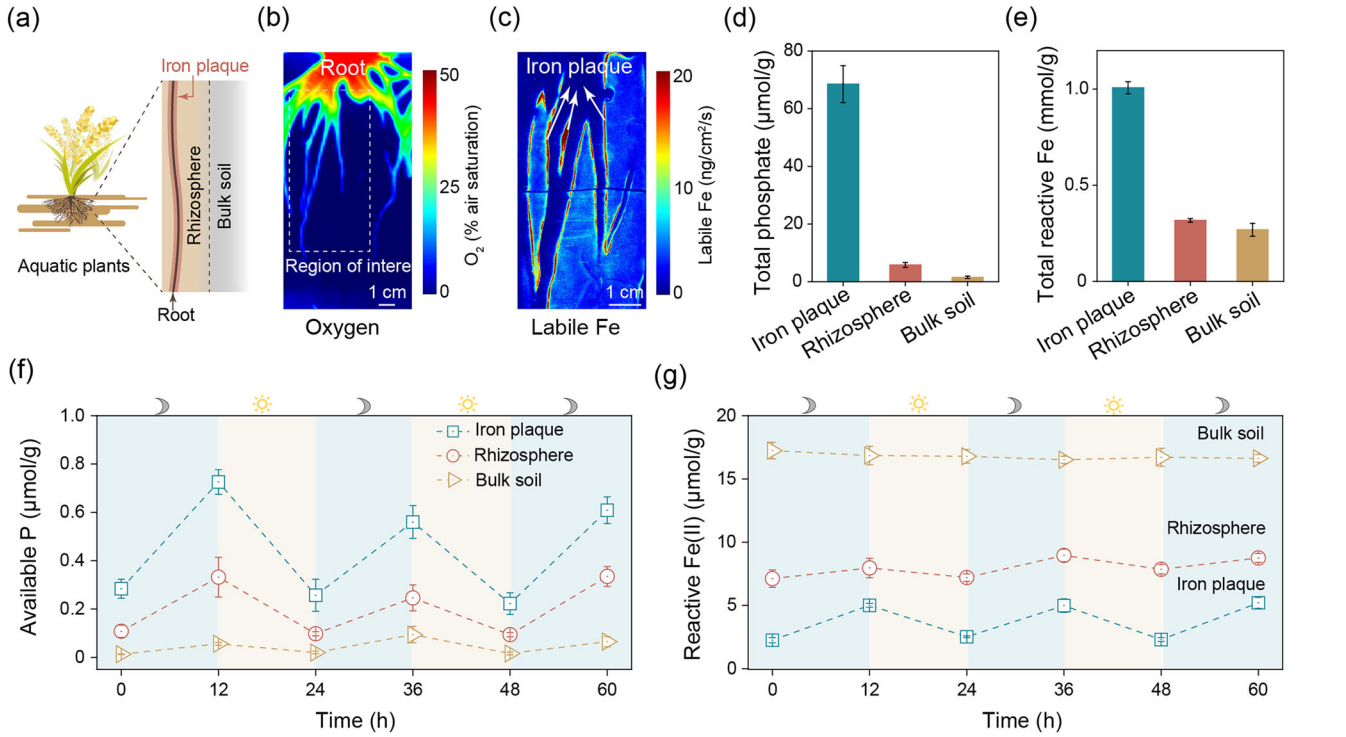

Fig. 3 | Reactive mineral phases (RMPs) regulate P mobilization around the roots. a Schematic representation of iron plaque, rhizosphere soil, and bulk soil surrounding the roots. **b**, **c** Aquatic roots exhibiting radial oxygen loss (ROL), with iron plaque adsorbed on the root surface within the region of interest. **d**, **e** Total phosphate and total reactive iron extracted from iron plaque, rhizosphere soil, and bulk soil using HCl. **f**, **g** Diel fluctuations of available P and reactive Fe(II) in iron plaque, rhizosphere soil, and bulk soil. The error bars represent the standard deviations of three replicates. When error bars are not visible, they are contained within the marker symbols.

iron mineral, widely distributed in soils and sediments[25]. To simulate rhizosphere redox conditions, the goethite was incubated under diel cycles of microbial reduction and air oxidation for 30 days. Mediated electrochemical analysis revealed that redox cycling significantly enhanced the redox reactivity of goethite. MER results showed increased reduction peaks after redox fluctuations, indicating enhanced reducibility, while MEO revealed pronounced oxidation peaks, absent before redox cycling, highlighting improved oxidizability (Fig. 4a). Integrating the current over time, the EEC of goethite after redox fluctuations was 57 mmol e^-/g, 1.6 times higher than that of goethite without redox activation (Fig. 4b). This enhanced redox reactivity is attributed to diel redox fluctuations, which facilitated the formation of more reactive secondary minerals on the goethite surface. XAS analysis revealed that these secondary minerals were primarily ferrihydrite (13%) and adsorbed Fe(II) ions (10%) (Fig. 4c). These results suggest that ROL-induced rapid redox turnover activates redox-inert crystalline iron phases, transforming them into redox-active RMPs.

To evaluate whether RMPs generated by redox oscillations enhance P accumulation and release, we exposed goethite, both before and after redox fluctuations, to a potassium dihydrogen phosphate solution. Adsorption kinetics revealed that redox-activated goethite (post-redox fluctuations) exhibited significantly greater phosphate adsorption efficiency compared to its unactivated counterpart (pre-redox fluctuations) (Fig. 4d). These findings suggest that RMPs formed through redox oscillations of highly crystalline iron minerals play a critical role in enhancing P accumulation. To further evaluate the impact of redox activation on phosphate release, we employed electrochemical reduction to compare the efficiency of phosphate release from goethite before and after redox fluctuations. Microbial reduction was avoided to eliminate potential interference from microbial phosphate uptake. A working electrode was fabricated by immobilizing sterilized goethite-bound phosphate (treated with NaN_3) onto conductive carbon paper, secured with a binding film to enable in-situ capture of released phosphate during reduction (Fig. 4e). The reduction potential was set to −0.21 V (vs. SHE), a condition representative of microbial electron transfer to Fe(III) at a similar potential[20]. Imaging results revealed that phosphate release efficiency from the reductive dissolution of redox-activated goethite was significantly higher than that of unactivated goethite (Fig. 4e). Similarly, Fe(II) generation in the electrolyte during reduction was markedly higher for redox-activated goethite compared to its unactivated counterpart (Fig. 4f). These results suggest that diel ROL-induced periodic redox turnover transforms redox-inert crystalline iron minerals into redox-active RMPs, which are highly effective in mediating both the accumulation and release of available P.

Ubiquity of ROL in enhancing P availability in the rhizosphere

We then investigated whether diel ROL could universally activate soil iron minerals, enhancing P availability across diverse plant communities and soils from intensively managed agricultural regions (Fig. 5a and Table S1). To simulate natural growth conditions, we incubated rice (a paddy-field species) and reed (a riparian wetland species), both aquatic plants, under flooded conditions, while wheat, a terrestrial xerophyte, was grown under drained conditions. Planar optode measurements revealed that, under flooded conditions, both rice and reed roots exhibited diel ROL activity, with dissolved oxygen concentrations around the roots increasing during the day and declining at night. In contrast, wheat, grown under non-flooded conditions, maintained an air-filled soil environment around its roots to support growth, showing no diel ROL fluctuations (Fig. 5b).

After the incubation, the roots of rice and reed, which exhibited diel ROL activity, developed distinct iron plaques on their surfaces, whereas the roots of wheat, lacking fluctuated ROL activity, did not

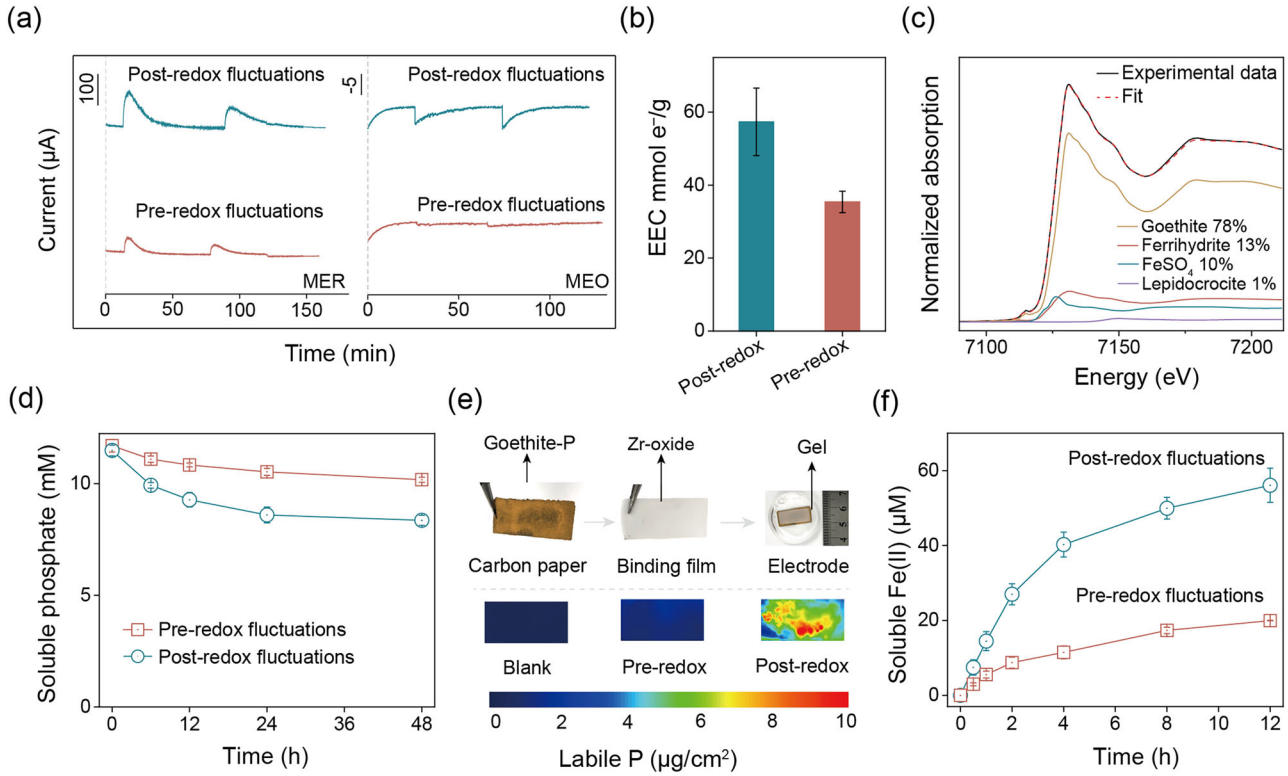

Fig. 4 | Radial oxygen loss (ROL)-induced redox alternations facilitate the generation of reactive mineral phases (RMPs). a, **b** Mediated electrochemical reduction (MER), mediated electrochemical oxidation (MEO), and electron exchange capacity (EEC) analyses of goethite before and after redox fluctuations. **c** Iron speciation of goethite following redox fluctuations, analyzed using X-ray absorption spectroscopy. **d** Comparison of phosphate adsorption kinetics on goethite before and after redox fluctuations. **e** Electrochemical reduction of redox-activated and untreated goethite with adsorbed phosphate (goethite-P). **f** Dissolved Fe(II) detected in the electrolyte during the electrochemical reduction of goethite with goethite-P. The error bars represent the standard deviations of three replicates. When error bars are not visible, they are contained within the marker symbols.

form iron plaques (Fig. S9). We then isolated the iron plaques from the roots, along with the rhizosphere and bulk soils, and analyzed the concentrations of available P and reactive iron. The results show that in rice and reed, the concentrations of available P and reactive iron were highest in the iron plaques, followed by the rhizosphere and bulk soils. In contrast, for wheat, the distribution of available P and reactive iron showed no spatial differences between the rhizosphere and bulk soils (Fig. 5c, d). Overall, these findings indicate that diel ROL in aquatic plants ubiquitously triggers the activation of soil iron minerals in the root zone, thereby enhancing P availability in the rhizosphere, whereas terrestrial plants lacking diel ROL fluctuations do not exhibit this effect.

Agricultural benefits of ROL in enhancing P availability

Using rice as a case study, we present a preliminary estimate of the global increase in available P in paddy fields driven by rhizospheric ROL activation. Based on our dataset, we developed a mathematical model (Eq. 1) to calculate the global distribution of ROL-activated P in rice paddies, with a spatial resolution of 5 arcmin (~10 km). The model is built on key assumptions, including ROL-activated P yield per unit soil mass, global paddy soil bulk density, harvested rice area, average rooting depth, and the rhizosphere soil volume fraction. This model provides a straightforward estimate of the potential global agricultural benefits of ROL in enhancing P availability. Our results indicate that global ROL-activated P for one year is approximately 0.2 million tons (Mt), with significant hotspots in South Asia, Southeast Asia, and Africa (Fig. 6a). This represents up to 8.7% of the total P fertilizer applied to global paddy fields (~2.3 Mt in 2021)[26]. We further quantified the distribution of the 0.2 Mt of activated P across different countries. The results in Fig. 6b indicate that ROL-activated P is primarily concentrated in major rice-growing regions, including India (29%), China (18%), Thailand (7%), Bangladesh (7%), and Indonesia (6%).

Based on the global market price of P fertilizer (521 USD/t, expressed as P_2O_5)[27], the activated P through rhizosphere ROL in rice paddies worldwide could generate an annual economic benefit of approximately 0.52 billion USD. The countries set to gain the most are India and China, with estimated benefits of 0.15 billion USD and 0.08 billion USD per year, respectively (Fig. 6c). In addition to rice, other aquatic plants also activate P in soils, potentially increasing the global economic value. Given the uneven economic development across regions, the application of P fertilizer in rice paddies varies globally. We next assessed the dependence on rhizosphere ROL-activated P in rice fields across different continents. In Africa, where P fertilizer application is limited, rice paddies primarily rely on the natural rhizosphere ROL process to mobilize soil P for crop growth, resulting in the highest dependence of 0.87 (Fig. 6d). While the global model provides valuable insights, it is based on several simplifying assumptions that introduce potential limitations. These include simplified representations of soil property heterogeneity, root architecture variability, and climate influences, which could affect model accuracy. Future improvements should incorporate higher-resolution data and region-specific parameters to reduce uncertainty.

In conclusion, we report a ubiquitous but previously overlooked diel ROL-induced redox fluctuation in the activation of thermodynamically stable iron minerals for enhanced P bioavailability in the rhizosphere. Notably, the periodic redox fluctuations induced by diel ROL play a crucial role in the formation of RMPs around the roots. These RMPs are highly redox-active and can efficiently shuttle available P from the soil into the rhizosphere porewater, driven by the alternation between daytime oxidation and nighttime reduction. In this

https://doi.org/10.1038/s41467-025-59637-x

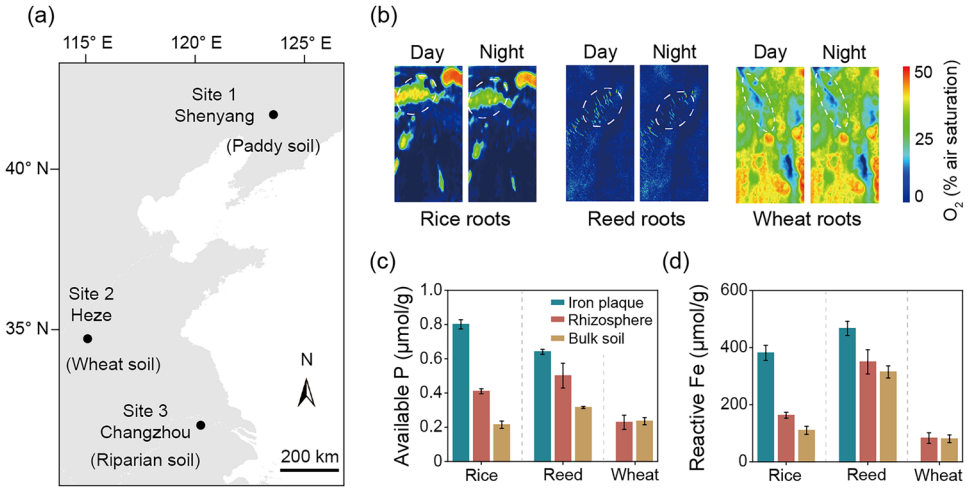

Fig. 5 | Radial oxygen loss (ROL)-mediated enhancement of available P by different plants. a Map showing soil and plant sampling locations. **b** Diel variation in oxygen concentration in the root zone of rice, reed, and wheat. **c**, **d** Available P and reactive iron concentrations in iron plaques, rhizosphere soil, and bulk soil of rice, reed, and wheat. The error bars represent the standard deviations of three replicates. When error bars are not visible, they are contained within the marker symbols.

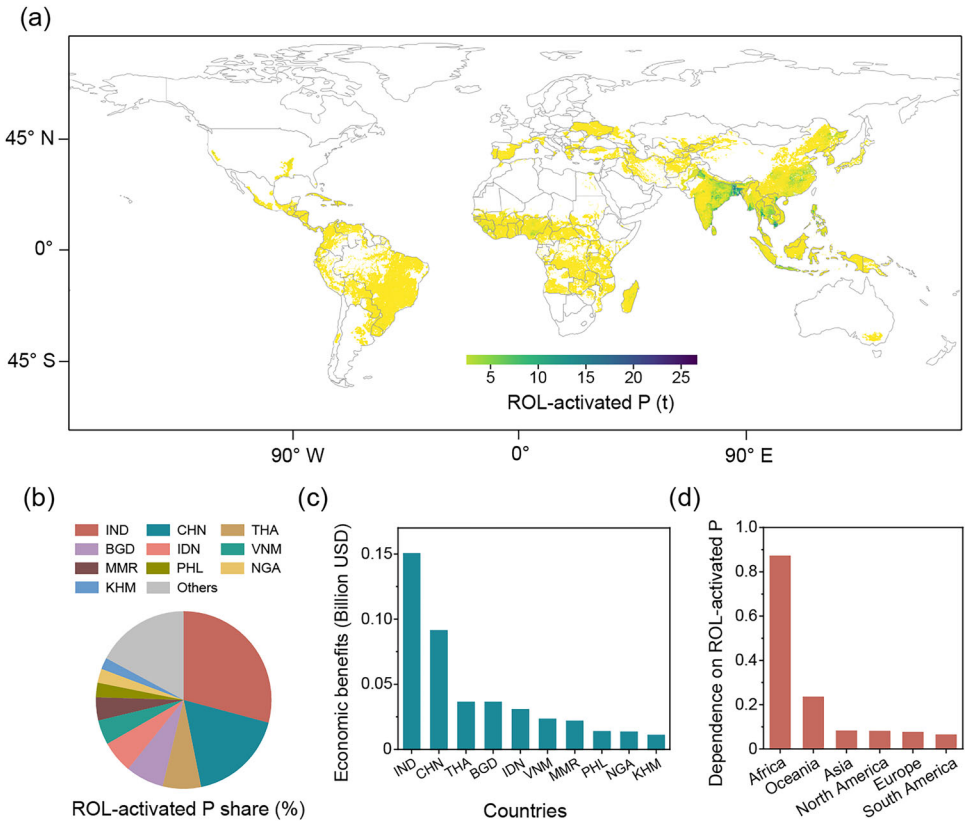

Fig. 6 | Global P benefits induced by radial oxygen loss (ROL) in paddy fields. a The geographical distribution of ROL-activated P in paddy fields. The data is based on the global harvest area of paddy fields, derived from a published global dataset[43], with a spatial resolution of 5 arcmin (~10 km). There are 463,429 points on this map at a 10 km × 10 km resolution. **b** Proportion of ROL-activated P in the top 10 countries globally. **c** Economic value of ROL-activated P in the top 10 countries globally. **d** Dependence on ROL-activated P in paddy fields across continents, defined as the proportion of total P input supplied by ROL-activated P.

context, regions characterized by frequent redox fluctuations (e.g., rhizosphere ecosystems[28], nearshore aquifers[29], paddy fields[30]) may serve as hotspots for RMP formation, facilitating the production of available P at localized interfaces where oxygen fluctuates for supporting plant growth.

Given that P controls the growth of crops in soil[31], our findings also offer implications for sustainable agricultural management. Improving alternate wetting and drying irrigation to induce frequent redox fluctuations may enhance the formation of RMPs in the soil, thereby improving the availability of legacy P for crop uptake. It is well-known that the preservation of organic carbon in soil is closely related to the speciation and reactivity of iron minerals[19,32]. Future research could also focus on the processes of the iron-carbon cycle and its associated impact on climate change at redox-fluctuating interfaces.

Methods

Cultivation and experimental setup

Seedlings of rice (*Oryza sativa* L.), macrophyte (*Vallisneria natans* H. and *Phragmites australis*), and winter wheat (*Triticum aestivum* L.) were transplanted into transparent rhizoboxes (30 × 10 × 5 cm, L × W × H) filled with either soil or aquatic sediment. Paddy soil was collected from a rice field in Shenyang, China (41.6°N, 123.3°E), wheat soil was sourced from a field in Heze, China (34.7°N, 115.6°E), and aquatic sediment was obtained from the riparian zone of the Yangtze River (31.9°N, 120.0°E). The physicochemical properties of these soils and sediments are detailed in Table S1. The rhizoboxes were maintained under flooded conditions in a controlled greenhouse for 30 days to establish equilibrium. Greenhouse conditions included a 12-h photoperiod with daytime temperatures of 28 °C and 70% relative humidity, and nighttime temperatures of 25 °C and 70% relative humidity. The light intensity was set to approximately 25 mW/cm². To prevent light exposure to roots, the rhizoboxes were wrapped in aluminum foil, and seedlings were positioned at a 45° angle to guide root growth along the removable window of the rhizobox (Fig. S1). Dissolved oxygen and redox potential in the root zone were measured in-situ using a planar optode and microelectrode sensors (Unisense, ROX-N; Science Park, Aarhus, Denmark). Detailed descriptions of these measurement techniques are provided in Section S1.

Imaging detection of labile P and soluble Fe(II)

The spatial distribution of labile P around the roots was visualized using DGT technology. DGT probes were prepared using an acrylamide gel (15%) with an agarose-derived cross-linker (0.3%) as the diffusion layer (0.8 mm thick), and a Zr-oxide gel (0.4 mm thick) as the binding layer, following established protocols[33]. After the pre-incubation period, the Zr-oxide gel was affixed to the inner wall of the detachable rhizobox, overlaid with the diffusive gel, and covered with a poly(-vinylidene fluoride) (PVDF) filter membrane (Whatman, 0.45 μm pore size). The PVDF membrane provided protection from soil particle abrasion while permitting the diffusion of available P from the soil surrounding the roots to the binding layer. Following a 12-h incubation under either light or dark conditions, the DGT probes were removed, rinsed with deionized water, and the binding layer was immersed in a color-developing solution containing molybdate and 10% ascorbic acid. The resulting labile P distribution was visualized by scanning the binding layer and performing grayscale transformation to generate an imaging map.

DET was employed to visualize the distribution of dissolved Fe(II) around the roots. The DET probes were fabricated using an acrylamide gel (15%) with an agarose-derived cross-linker (0.3%) as the diffusion layer[34]. The diffusion gel (0.8 mm thick) was affixed directly to the inner wall of the detachable rhizobox and covered with a PVDF filter membrane (Whatman, 0.45 μm pore size) to allow the diffusion of soluble Fe(II) while protecting the gel from soil particle abrasion. After the incubation period, the diffusion gel was removed, rinsed with deionized water, and immersed in a 1,10-phenanthroline solution (0.5%) to visualize Fe(II). The distribution of dissolved Fe(II) was captured by scanning the gel, followed by grayscale transformation to generate an imaging map.

Sampling iron plaque, rhizosphere soil, and bulk soil

Iron plaque on root surfaces was extracted using an ultrasonic detachment method[35]. In brief, roots bearing visible iron plaque were first cleaned of loosely attached soil by gentle shaking, then immersed in 100 mL of ultrapure water in a round-bottom flask. The roots were subjected to ultrasonication for 2 h at room temperature to dislodge the iron plaque. The resulting suspension was vacuum-filtered through a PVDF filter membrane (Whatman, 0.2 μm pore size). The filter membrane was subsequently lyophilized, and the powder recovered from the membrane was designated as iron plaque. Rhizosphere soil, defined as soil within 4 mm of the root surface[36,37], was collected by gently detaching soil from the roots using a soft brush and shaking. Bulk soil, defined as soil located more than 2 cm from the roots[38], was sampled from each plot to serve as a control.

Electrochemical analysis

Cyclic voltammetry (CV) was performed using a CHI 660 electrochemical workstation equipped with a sealed H-type cell separated by a Nafion-117 proton exchange membrane. An Ag/AgCl electrode with a salt bridge and a platinum mesh served as the reference and counter electrodes, respectively. To prepare the working electrode, lyophilized samples (10 mg) were dispersed in a solution of 50 μL Nafion (5 wt%) and 950 μL ethanol, followed by sonication for 10 min. The resulting suspension was drop-cast onto carbon paper (Sigracet 29BC, Germany) with a 1 × 1 cm² active area and dried at 30 °C. Electrochemical measurements were conducted in Ar-saturated KCl (0.1 M) and MOPS buffer (10 mM, pH 7.0) as electrolytes. CV spectra were recorded in the potential range of 0.61 to −0.45 V vs. the standard hydrogen electrode (SHE) at a scan rate of 10 mV/s, consistent with the redox potential typically observed in soils[39]. All potentials referenced to Ag/AgCl (saturated KCl) were converted to the SHE scale by adding +0.197 V[40].

The EEC of the samples was determined using a mediated electrochemical method[41]. A coiled platinum wire with a porous glass frit served as the counter electrode, while an Ag/AgCl electrode was used as the reference. The working electrode and electrochemical cell were combined in a 9 mL glassy carbon beaker (Sigradur G, HTW, Germany). Electrochemical measurements were conducted in Ar-saturated KCl (0.1 M) and MOPS buffer (10 mM, pH 7.0) as electrolytes. MEO and MER were performed in an anoxic glovebox with N_2 atmosphere (O_2 < 0.1 ppm, Mikrouna, China). 2,2′-azino-bis(3-ethylbenzothiazoline-6-sulfonic acid) (ABTS) and ethyl viologen dibromide (EtV) were employed as electron transfer mediators for MEO and MER, respectively. The applied redox potentials were set to 0.61 V and −0.45 V vs. SHE for MEO and MER, respectively. The number of electrons transferred to or from the post-reaction samples was quantified by integrating the reductive and oxidative current responses in the i–t (current-time) curves of MEO and MER (Section S3).

Determination of available P and reactive Fe

Available P in iron plaque, rhizosphere soil, and bulk soil was quantified using the Olsen P method[24]. Lyophilized samples (1.0 g) were added to 50-mL centrifuge tubes, followed by the addition of 20 mL of 0.5 M bicarbonate solution (pH 8.5) as the extractant and shaken for 30 min. The concentration of available P in the extracts was determined by measuring absorbance at 700 nm using the molybdenum blue method.

Reactive iron in the samples was extracted using hydrochloric acid (HCl) and analyzed following the 1,10-phenanthroline method[42]. For this, lyophilized samples (1.0 g) were suspended in 20 mL of 1 M HCl and shaken for 24 h. Reactive Fe(II) in the extracts was quantified by measuring absorbance at 510 nm using the 1,10-phenanthroline method. Total reactive iron was determined by measuring the absorbance of ferrous complexes formed with 1,10-phenanthroline after the addition of hydroxylamine hydrochloride as a reducing agent.

Activation of goethite through redox fluctuations

To explore the formation mechanisms of RMPs under diel redox fluctuations, highly crystalline goethite was subjected to alternating microbial reduction and oxygen-driven oxidation cycles over a 30-day period. Specifically, 40 mg of goethite was added to 40 mL of *Shewanella oneidensis* strain MR-1 culture solutions (1×10^8 cells/mL), containing 20 mM lactate and 50 mM Tris-HCl buffer (pH 7.0). The suspensions were initially incubated anaerobically in the dark at 28 °C for 5 days to establish equilibrium. Following preincubation, the system was exposed to air and illuminated (25 mW/cm²) for 12 h at 28 °C to simulate daytime rhizosphere oxidation. This was followed by

deoxygenation with high-purity N_2 and incubation in the dark at 25 °C for 12 h to mimic nocturnal rhizosphere reduction. The temperatures of 28 °C and 25 °C reflect typical diurnal fluctuations in flooded rice paddies. These diel redox cycles were repeated for 30 days. Upon completion, the redox-oscillation-activated goethite was washed with ultrapure water and lyophilized for subsequent analysis.

Redox-activated goethite governs P mobilization

To assess the P accumulation capacity of goethite, both redox-activated and unactivated, potassium dihydrogen phosphate (12 mM) was added to 20 mL suspensions of goethite (2 g/L) prepared before and after redox fluctuations. At designated time intervals, aliquots (500 µL) were collected and filtered through a 0.45 µm membrane for soluble phosphate analysis using the molybdenum blue method.

Following P adsorption, the precipitates were recovered by centrifugation, washed, and lyophilized to obtain goethite-associated P (goethite-P). Electrochemical reduction was employed to compare the efficiency of phosphate release from goethite-P. The reduction process was conducted in a sealed H-type cell separated by a proton exchange membrane (Nafion-117). A silver/silver chloride (Ag/AgCl) electrode with a salt bridge and a platinum mesh electrode served as the reference and counter electrodes, respectively. A custom-developed conductive imaging gel film embedded with goethite-P was used as the working electrode (Section S8). The electrolyte consisted of argon-saturated KCl (0.1 M) supplemented with MOPS buffer (10 mM, pH 7.0). The reduction was carried out at a redox potential of −0.21 V vs. the standard hydrogen electrode (SHE) for 12 h. During the process, 0.5 mL of the electrolyte was sampled at predetermined time points to measure Fe(II) concentrations using the 1,10-phenanthroline method. Following the reduction, the binding layer was immersed in a solution containing molybdate and 10% ascorbic acid, and an imaging map of the released phosphate was obtained through scanning and grayscale transformation.

Global mapping of ROL-activated P in paddy soils

To quantify the benefits of ROL-activated P in the rhizosphere, we propose an ROL-P estimator model to assess the increase in available P in rice paddies driven by ROL (Eq. 1).

$$\Delta m_P = \left[\Delta c_P \cdot M_P\right] \cdot \left[\rho_s \cdot A_h \cdot d_s \cdot \gamma_r\right] \quad (1)$$

where Δm_P represents the mass of ROL-activated P over the course of one year (kg P). Δc_P represents the concentration of ROL-activated P in rhizosphere soil per unit mass during a rice-growing season (µmol/g soil); Δc_P is calculated as the difference between the average available P concentration in the iron plaque and rhizosphere soil, and the available P concentration in the bulk soil (Section S10). M_P is the molar mass of P (3.1×10^{-8} kg P/µmol). ρ_s refers to the bulk density of paddy soil (g soil/m^3), which is derived from the Harmonized World Soil Database Version 2.0 (2023). Ah is the harvest area of the paddy field (m^2), based on reported data[43]. d_s is the tillage depth of the paddy field (typically 0.2 m)[44]. γ_r represents the proportion of rhizosphere volume relative to the total soil volume, with a reported value of 5%[45]. The calculation of the economic benefits and dependency on ROL-activated P are presented in sections S11 and S12, respectively.

Data availability

All data generated or analyzed during this study are included in this published article (and its supplementary information files). Source data are provided with this paper.

References

1. Gamuyao, R. et al. The protein kinase Pstol1 from traditional rice confers tolerance of phosphorus deficiency. *Nature* **488**, 535–539 (2012).
2. Han, M. et al. Root phosphatase activity aligns with the collaboration gradient of the root economics space. *New Phytol.* **234**, 773–775 (2021).
3. Chen, X., Chen, H. Y. H. & Chang, S. X. Meta-analysis shows that plant mixtures increase soil phosphorus availability and plant productivity in diverse ecosystems. *Nat. Ecol. Evol.* **6**, 1112–1121 (2022).
4. Sakuraba, Y. et al. A phytochrome-B-mediated regulatory mechanism of phosphorus acquisition. *Nat. Plants* **4**, 1089–1101 (2018).
5. Fang, W. et al. Combining multiple high-resolution in situ techniques to understand phosphorous availability around rice roots. *Environ. Sci. Technol.* **55**, 13082–13092 (2021).
6. Shi, J. et al. A phosphate starvation response-centered network regulates mycorrhizal symbiosis. *Cell* **184**, 5527–5540 (2021).
7. Guo, L. et al. Acceleration of phosphorus weathering under warm climates. *Sci. Adv.* **10**, eadm7773 (2024).
8. Brodersen, K. E. et al. Seagrass-mediated phosphorus and iron solubilization in tropical sediments. *Environ. Sci. Technol.* **51**, 14155–14163 (2017).
9. Zhao, W. et al. Chemical speciation of phosphorus in farmland soils and soil aggregates around mining areas. *Geoderma* **433**, 116465 (2023).
10. Colombo, C., Palumbo, G., He, J.-Z., Pinton, R. & Cesco, S. Review on iron availability in soil: interaction of Fe minerals, plants, and microbes. *J. Soil Sediment* **14**, 538–548 (2014).
11. Chen, N. et al. Active iron phases regulate the abiotic transformation of organic carbon during redox fluctuation cycles of paddy soil. *Environ. Sci. Technol.* **55**, 14251–14293 (2021).
12. Aeppli, M. et al. Decreases in iron oxide reducibility during microbial reductive dissolution and transformation of ferrihydrite. *Environ. Sci. Technol.* **53**, 8736–8746 (2019).
13. Aeppli, M. et al. Electrochemical analysis of changes in iron oxide reducibility during abiotic ferrihydrite transformation into goethite and magnetite. *Environ. Sci. Technol.* **53**, 3568–3578 (2019).
14. Schulz, K. et al. Iron oxyhydroxide transformation in a flooded rice paddy field and the effect of adsorbed phosphate. *Environ. Sci. Technol.* **58**, 10601–10610 (2024).
15. Zhao, K., Ma, B., Xu, Y., Stirling, E. & Xu, J. Light exposure mediates circadian rhythms of rhizosphere microbial communities. *ISME J.* **15**, 2655–2664 (2021).
16. Wu, B. et al. Radial oxygen loss triggers diel fluctuation of cadmium dissolution in the rhizosphere of rice. *Environ. Sci. Technol.* **58**, 14718–14725 (2024).
17. Dai, H. et al. Dynamic in situ detection in iRhizo-Chip reveals diurnal fluctuations of Bacillus subtilis in the rhizosphere. *Proc. Natl. Acad. Sci. USA* **121**, e2408711121 (2024).
18. McRose, D. L. & Newman, D. K. Redox-active antibiotics enhance phosphorus bioavailability. *Science* **371**, 1033–1037 (2021).
19. Dong, H. et al. Coupled iron cycling and organic matter transformation across redox interfaces. *Nat. Rev. Earth. Environ.* **4**, 659–673 (2023).
20. Aeppli, M., Thompson, A., Dewey, C. & Fendorf, S. Redox properties of solid phase electron acceptors affect anaerobic microbial respiration under oxygen-limited conditions in floodplain soils. *Environ. Sci. Technol.* **56**, 17462–17470 (2022).
21. Sheng, A. et al. Labile Fe(III) from sorbed Fe(II) oxidation is the key intermediate in Fe(II)-catalyzed ferrihydrite transformation. *Geochim. Cosmochim. Acta* **272**, 105–120 (2020).
22. Peiffer, S. et al. A biogeochemical-hydrological framework for the role of redox-active compounds in aquatic systems. *Nat. Geosci.* **14**, 264–272 (2021).
23. van Bodegom, P. M., van Reeven, J. & Denier van der Gon, H. A. C. Prediction of reducible soil iron content from iron extraction data. *Biogeochemistry* **64**, 231–245 (2003).

24. Wang, Y. et al. Reduced phosphorus availability in paddy soils under atmospheric CO_2 enrichment. *Nat. Geosci.* **16**, 162–168 (2023).
25. Basinski, J. J. et al. Unraveling iron oxides as abiotic catalysts of organic phosphorus recycling in soil and sediment matrices. *Nat. Commun.* **15**, 5930 (2024).
26. Coello, F. et al. Global Crop-specific fertilization dataset from 1961–2019. *Sci. Data* **12**, 40 (2025).
27. World bank commodity markets outlook. https://www.worldbank.org/en/research/commodity-markets (2021).
28. Zhu, G. et al. Hotspots of anaerobic ammonium oxidation at land–freshwater interfaces. *Nat. Geosci.* **6**, 103–107 (2013).
29. van Erk, M. R. et al. Reactive oxygen species affect the potential for mineralization processes in permeable intertidal flats. *Nat. Commun.* **14**, 938 (2023).
30. Dai, H., Wu, B., Chen, B., Ma, B. & Chu, C. Diel fluctuation of extracellular reactive oxygen species production in the rhizosphere of rice. *Environ. Sci. Technol.* **56**, 9075–9082 (2022).
31. Duhamel, S. The microbial phosphorus cycle in aquatic ecosystems. *Nat. Rev. Microbiol.* **23**, 239–255 (2025).
32. Patzner, M. S. et al. Iron mineral dissolution releases iron and associated organic carbon during permafrost thaw. *Nat. Commun.* **11**, 6329 (2020).
33. Ding, S., Wang, Y., Xu, D., Zhu, C. & Zhang, C. Gel-based coloration technique for the submillimeter-scale imaging of labile phosphorus in sediments and soils with diffusive gradients in thin films. *Environ. Sci. Technol.* **47**, 7821–7829 (2013).
34. Robertson, D., Teasdale, P. R. & Welsh, D. T. A novel gel-based technique for the high resolution, two-dimensional determination of iron (II) and sulfide in sediment. *Limnol. Oceanogr. Meth.* **6**, 502–512 (2008).
35. Amaral, D. C., Lopes, G., Guilherme, L. R. G. & Seyfferth, A. L. A new approach to sampling intact Fe plaque reveals Si-induced changes in Fe mineral composition and shoot as in rice. *Environ. Sci. Technol.* **51**, 38–45 (2017).
36. Domeignoz-Horta, L. A. et al. Plant diversity drives positive microbial associations in the rhizosphere enhancing carbon use efficiency in agricultural soils. *Nat. Commun.* **15**, 8065 (2024).
37. Kuzyakov, Y. & Razavi, B. S. Rhizosphere size and shape: temporal dynamics and spatial stationarity. *Soil. Biol. Biochem.* **135**, 343–360 (2019).
38. Tang, X. et al. Long-term manure application changes bacterial communities in rice rhizosphere and arsenic speciation in rice grains. *Environ. Sci. Technol.* **55**, 1555–1565 (2021).
39. Zhang, Y. et al. Directional long-distance electron transfer from reduced to oxidized zones in the subsurface. *Nat. Commun.* **15**, 6576 (2024).
40. Li, X.-R. et al. In situ studies of hydrogen evolution kinetics on pure titanium surface: the effects of pre-reduction and dissolved oxygen. *J. Phys. Chem. C.* **126**, 1828–1844 (2022).
41. Kluepfel, L., Piepenbrock, A., Kappler, A. & Sander, M. Humic substances as fully regenerable electron acceptors in recurrently anoxic environments. *Nat. Geosci.* **7**, 195–200 (2014).
42. Wallmann, K., Hennies, K., Konig, I., Petersen, W. & Knauth, H. D. New procedure for determining reactive Fe(III) and Fe(II) minerals in sediments. *Limnol. Oceanogr.* **38**, 1803–1812 (1993).
43. Xie, H. et al. GloRice, a global rice database (v1.0): I. Gridded paddy rice annual distribution from 1961 to 2021. *Sci. Data* **12**, 182 (2025).
44. Barison, J. & Uphoff, N. Rice yield and its relation to root growth and nutrient-use efficiency under SRI and conventional cultivation: an evaluation in Madagascar. *Paddy Water Environ.* **9**, 65–78 (2011).
45. Wei, X. et al. Expansion of rice enzymatic rhizosphere: temporal dynamics in response to phosphorus and cellulose application. *Plant Soil* **445**, 169–181 (2019).

Acknowledgements

This work was supported by the National Key Research and Development Plan (2024YFC3211100, S.D.), the National Natural Science Foundation of China (NSFC, 42407535, C.L.; 42107392, G.Z.; 52479079, H.X.), the State Key Laboratory of Lake and Watershed Science for Water Security (NKL2023-QN01, G.Z.; NKL2023-QN05, H.S.), the Natural Science Foundation of Jiangsu Province (BK20241697, C.L.), the Postdoctoral Fellowship Program of the China Postdoctoral Science Foundation (CPSF, GZB20230782, 2024M763366, C.L.), the Key Research and Development Program of Jiangsu Province (BE2023846, H.X.), and the Major Science and Technology Project of Yunnan Province (202202AE090034, H.S.). We thank the BL11B beamline at the Shanghai Synchrotron Radiation Facility (https://cstr.cn/31124.02.SSRF.BL11B) for their support with the X-ray absorption spectroscopy measurements.

Author contributions

G.Z. and C.L. designed the study; C.L., M.T., and H.D. cultivated the plants; C.L. prepared the imaging gels and planar optoelectronics; G.Z. conducted the electrochemical experiments and fabricated the imaging electrode; H.S. conducted a global analysis of the distribution and benefits of ROL-activated P in rice paddy soils. M.T. and G.Z. collected soil samples; G.Z. wrote and revised the paper; X.W., H.X., and S.D. discussed the results and commented on the manuscript.

Competing interests

The authors declare no competing interests.

Additional information

Supplementary information The online version contains supplementary material available at https://doi.org/10.1038/s41467-025-59637-x.

Correspondence and requests for materials should be addressed to Guoqiang Zhao.

Peer review information *Nature Communications* thanks the anonymous reviewers for their contribution to the peer review of this work. A peer review file is available.